

<https://doi.org/10.1038/s42005-024-01569-x>

# Electromagnetic near-field mutual coupling suppression with active Janus sources

Check for updates

Bo Xue<sup>1</sup>, Kayode Adedotun Oyesina<sup>1</sup> & Alex M. H. Wong<sup>1,2</sup> ✉

Electric dipoles and magnetic dipoles are the most fundamental particles in electromagnetic theory. Huygens and Janus sources, formed by the orthogonal combination of electric and magnetic dipoles, both show good directionality in the near field. Although the Huygens source has been widely used in antennas and metasurfaces, the applications of Janus source are heretofore limited. In this paper we report the physical construction of an active Janus source. Through full-wave simulations within the parallel plate waveguide (PPW) environment, we show that our source achieves the directional electromagnetic near-field and quasi-isotropic far-field requisite of the Janus source. Using this fact, we demonstrate that two active Janus and Huygens sources in close proximity (about 0.10 to 0.25 wavelengths) achieve a near 1000-fold reduced mutual coupling compared to electric dipole sources. Particularly, the simultaneous achievement of strong mutual coupling suppression and quasi-isotropic radiation make the Janus source an ideal candidate for consideration in future compact multi-input multi-output (MIMO) communication systems.

Electric and magnetic dipoles, the fundamental sources of electromagnetic waves, by themselves produce omnidirectional radiation in the plane perpendicular to the dipole. However, their simple combinations quickly result in intricate directionalities of wide-ranging interest to physics, photonics and engineering. It is well known that a pair of co-located electric and magnetic dipoles, equal in radiation strength and phase and orthogonally directed in space, form a Huygens source which produces unidirectional radiation. This radiation characteristic was first described by Fresnel in his introduction of the obliquity factor<sup>1</sup>. Though at the time the reason for its occurrence was unknown, its introduction reconciles Huygens' wave theory of light with experimental observations. Through later developments from Kirchhoff<sup>2</sup>, Love<sup>3</sup> and Schelkunoff<sup>4</sup> we now understand that the obliquity factor occurs as a consequence of directive radiation of the Huygens sources that one obtains when one replaces a propagating plane wave with its secondary (or equivalent) sources along a constant phase plane. The unidirectional property of the Huygens source has been extensively studied, and passive and active Huygens sources find applications in various fields. Passive Huygens sources are used to attain flexible control of coupling direction to achieve directionality modulation<sup>5-7</sup>; Huygens metasurfaces are proposed to achieve flexible modulation of electromagnetic waves with high efficiency<sup>8-11</sup>. In the field of antennas, the magnetoelectric (ME) dipole<sup>12,13</sup> and the electrically small Huygens source antennas<sup>14,15</sup> use a combination of

electric and magnetic dipoles to construct high gain antennas leveraging the far-field directionality of Huygens source.

While the Huygens source achieves directionality in the far-field, a recently proposed Janus source achieves directionality in the near-field<sup>5</sup>. The Janus source features an electric and magnetic dipole pair which are co-located, orthogonally directed and with equal radiation strength, just like the Huygens source. However, in departure from the Huygens source, the electric and magnetic dipoles are shifted in phase by 90 degrees. Picardi et al. investigates parity and time-reversal of the circular, Huygens and Janus dipoles, and find that they possess distinct and unique directionalities in the near-field<sup>5</sup>. Hence the Janus dipole, like its Huygens' counterpart, can be used to build near-field directional devices – which has received strong recent interest with wide-ranging intended applications in power transfer, optical integrated circuits (IC) and molecule trapping<sup>5-7,16-22</sup>. Directional “meta-particles” have also been used to build metasurfaces yielding functionalities including wavefront manipulation, cloaking and wireless power transmission<sup>23-25</sup>. These works demonstrate the power of building devices and surfaces with a directional meta-particle – areas to which the Janus dipole has untapped potential to make unique contributions.

Recent works show important applications Janus sources have in near-field power coupling scenarios<sup>5,16-19,26-34</sup>. However, these works either treat the Janus source from a theoretical perspective with an ideal current

<sup>1</sup>Department of Electrical Engineering, City University of Hong Kong, Tat Chee Avenue, Kowloon, Hong Kong SAR, China. <sup>2</sup>State Key Laboratory of Terahertz and Millimeter Waves, City University of Hong Kong, Tat Chee Avenue, Kowloon, Hong Kong SAR, China. ✉e-mail: alex.mh.wong@cityu.edu.hk

doublet<sup>5,17,26,31,33</sup>, or employ a passive source, such as a nanosphere<sup>27</sup>, dielectric cylinder<sup>18</sup> or helix<sup>19</sup>, which scatters a very small fraction of an incident wave in a manner similar to a Janus source. Hence passive Janus sources are excited with limited power efficiency, which somewhat limits the possibility of their practical application. Further, requirement of an incident illumination, and the background EM field and scattering caused by it, forms spurious fields that are often undesirable. An active Janus source, which generates the desired electric and magnetic currents in the correct amplitude, phase and orientation, would be very desirable toward the experimental investigation and practical application of Janus sources. In addition, the active Janus source is more efficient and the modulation is more flexible compared to the passive Janus source.

One potential application of the Janus source is in closely spaced multi-input multi-output (MIMO) antenna systems. Having multiple closely spaced antennas can increase the capacity of the communication system, but the electromagnetic near-fields of these antennas often interfere with one another, resulting in performance degradation of various kinds<sup>35–37</sup>. Complicated decoupling networks are designed to suppress mutual coupling with varying degrees of success<sup>38–42</sup>. Pattern diversity method has also been used by employing antennas with different radiation patterns<sup>43–47</sup>. In this manner, mutual coupling can be reduced, but the communication performance may have angular variations. For example, for a MIMO antenna system transmitting two channels of information with different antenna patterns, the corresponding receivers may have dominant reception of either Channel A or Channel B, depending on their angular location with respect to the transmitter. Since the Janus source features near-field directionality while it possesses a near-isotropic far-field pattern, it has potential to suppress mutual coupling in a compact MIMO antenna system without compromising the radiation properties of individual antennas.

In this paper, we address the aforementioned scenarios by demonstrating (i) a practical active Janus source, and (ii) the significant

suppression of mutual coupling using active Janus sources. We experimentally report, to the best of our knowledge, the first realistic active Janus source, which we achieve by properly tuning the current running through two filaments placed within a parallel-plate metallic waveguide. This source can be generated by feeding two monopole antennas with a relatively simple microwave circuit. We then demonstrate that, when two such sources are placed within close proximity (from 0.08 to 0.24 wavelengths), the mutual coupling between them is reduced around 1000-fold compared to two dipoles of similar proximity. Our findings show that the Janus source can be excited in an active manner, with high power efficiency and without affecting the neighbouring sources, and that they can be used to suppress mutual coupling between two radiators in-close proximity to one-another. The work paves way to power-efficient active directional near-field power-coupling devices and opens doors to a new kind of compact MIMO antenna systems.

## Results

### Active Janus source

We introduce a 2D environment in which we investigate and demonstrate the active Janus source. Fig. 1a shows a parallel plate waveguide (PPW) environment with two perfect conductors normal to the  $z$ -direction. When separated at a distance  $h < \lambda/2$ , where  $\lambda$  is the electromagnetic wavelength, this environment only supports modes with non-zero  $\{H_x, H_y, E_z\}$ . All fields remain invariant in the  $z$ -direction, hence the effective 2D environment is constructed. Performing our investigation in a 2D (PPW) environment helps simplify our analysis. The conclusion from this work is nonetheless directly applicable to a 3D environment.

We have shown in earlier works<sup>11,34,48,49</sup> that the twin current filament (TCF) source shown in the inset of Fig. 1a can generate co-located, spatially orthogonal electric and magnetic current pairs in this environment. Essentially, when the current filaments are separated by a distance much

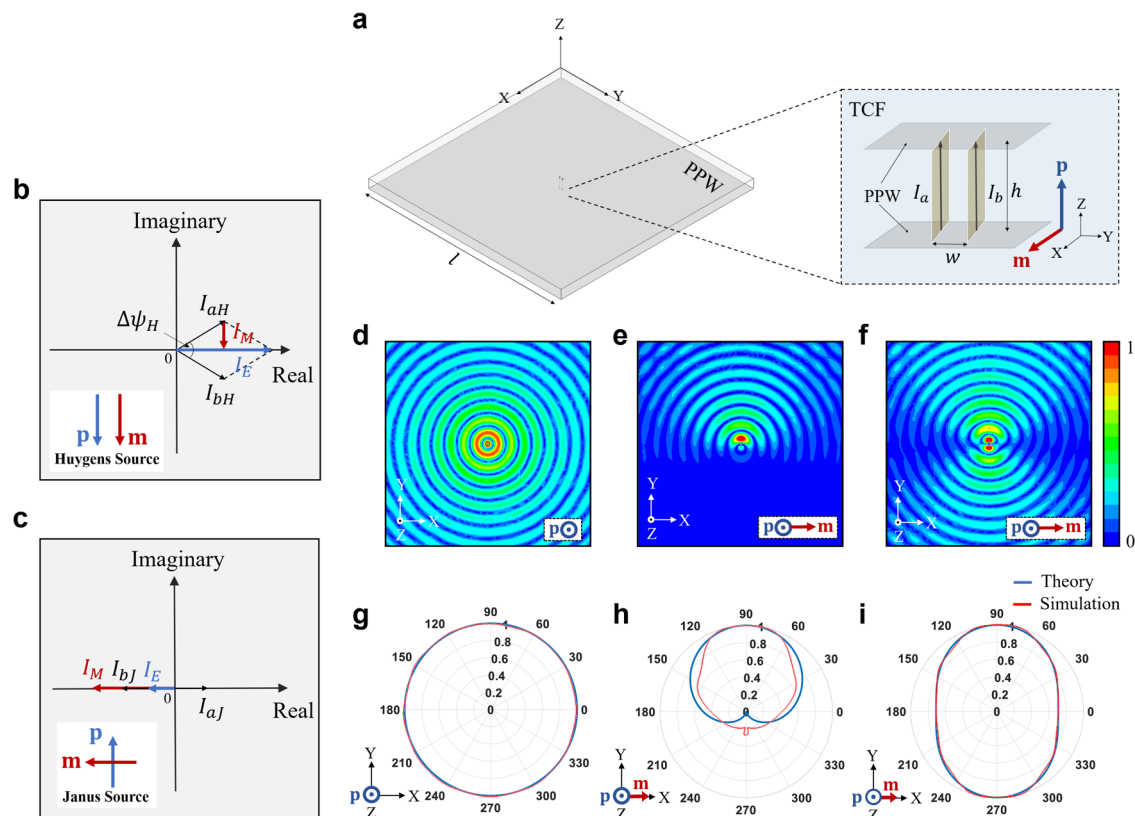


**Fig. 1 | Twin current filament (TCF) model and far-field characteristic.** **a** A diagram of the TCF model within the parallel plate waveguide (PPW).  $h = 45$  mm ( $0.12\lambda_0$ ),  $w = 15$  mm ( $0.04\lambda_0$ ) and simulations are performed at 800 MHz. **b, c** Argand diagrams of (b) the Huygens source and (c) the Janus source. **d–f** Simulated

normalized  $|E|$  within the PPW in the area surrounding (d) the electric dipole, (e) the Huygens source and (f) the Janus source. **g–i** Calculated radiation patterns of (g) the electric dipole, (h) the Huygens source and (i) the Janus source. The lower right of each subfigure shows the orientation of the electric and magnetic dipole moments.

smaller than the wavelength ( $w \ll \lambda$ ), they form an effective electric current  $I_E$  in the z-direction that is the sum of the currents flowing in both filaments. Conversely, an effective current loop  $I_M$  is formed with the difference of currents flowing in the filaments, which functions as an effective magnetic current in the yz-plane. Mathematically,

$$\begin{aligned} I_E &= I_b + I_a \\ I_M &= \frac{1}{2}(I_b - I_a) \end{aligned} \quad (1)$$

where  $I_a$  and  $I_b$  are electric currents flowing through the two filaments.

Following Eq. (1), a pure electric current source can be generated with  $I_a = I_b$ , while a pure magnetic current source can be generated with  $I_a = -I_b$ . More complicated superpositions can be achieved by properly tuning  $I_a$  and  $I_b$ . Particularly, the Huygens and Janus sources can be generated by requiring that the resultant magnetic and electric dipole moments  $\mathbf{m}$  and  $\mathbf{p}$  possess the same radiation strength and are either in phase (Huygens source) or phase-shifted by  $90^\circ$  (Janus source). The relationship between  $\{I_E, I_M\}$  and  $\{\mathbf{p}, \mathbf{m}\}$  is

$$\begin{aligned} \mathbf{p} &= \frac{I_E h}{j\omega} \hat{\mathbf{z}} \\ \mathbf{m} &= wh I_M \hat{\mathbf{x}} \end{aligned} \quad (2)$$

In Supplementary Note 1 we overview the derivation relating the electric and magnetic currents to the infinitesimal electric dipole and infinitesimal electric loop. From this, we can find the superposition of the electric dipole and electric loop currents that will give rise to the appropriate  $\mathbf{p}$  and  $\mathbf{m}$  which forms a Huygens and/or a Janus source. Applying Eq. (1) to equations (S3) and (S4) from Supplementary Note 1, we find that the Huygens and Janus sources can be generated when

$$\frac{I_{bH}}{I_{aH}} = -\frac{2h + jkA}{2h - jkA} = -\frac{1 + j\pi\left(\frac{w}{\lambda}\right)}{1 - j\pi\left(\frac{w}{\lambda}\right)} \quad (3)$$

for the Huygens source, and

$$\frac{I_{bj}}{I_{aj}} = -\frac{h + 2kA}{h - 2kA} = -\frac{1 + \pi\left(\frac{w}{\lambda}\right)}{1 - \pi\left(\frac{w}{\lambda}\right)} \quad (4)$$

for the Janus source.

We introduce a single excitation current  $I_0$ , for which

$$|I_0|^2 = |I_a|^2 + |I_b|^2; \Delta\psi = |\psi_b - \psi_a| \quad (5)$$

where the  $\psi_n$  is the phase of current excitation  $I_n$  ( $n = a, b$ ). Using Eq. (5) we rewrite the excitation conditions for the electric, Huygens and Janus dipoles as

$$I_{aE} = I_{bE} = \frac{1}{\sqrt{2}} I_0; \Delta\psi_E = 0; \quad (6)$$

for the electric dipole,

$$I_{aH} = \frac{1}{\sqrt{2}} I_0 e^{j\text{atan}(\xi^{-1})}; I_{bH} = \frac{1}{\sqrt{2}} I_0 e^{-j\text{atan}(\xi^{-1})}; \Delta\psi_H = 2\text{atan}(\xi^{-1}); \quad (7)$$

for the Huygens source, and

$$I_{aj} = \frac{1 - \xi}{\sqrt{2(1 + \xi^2)}} I_0; I_{bj} = -\frac{1 + \xi}{\sqrt{2(1 + \xi^2)}} I_0; \Delta\psi_j = \pi, \text{ where } \xi = \frac{\pi w}{\lambda} \quad (8)$$

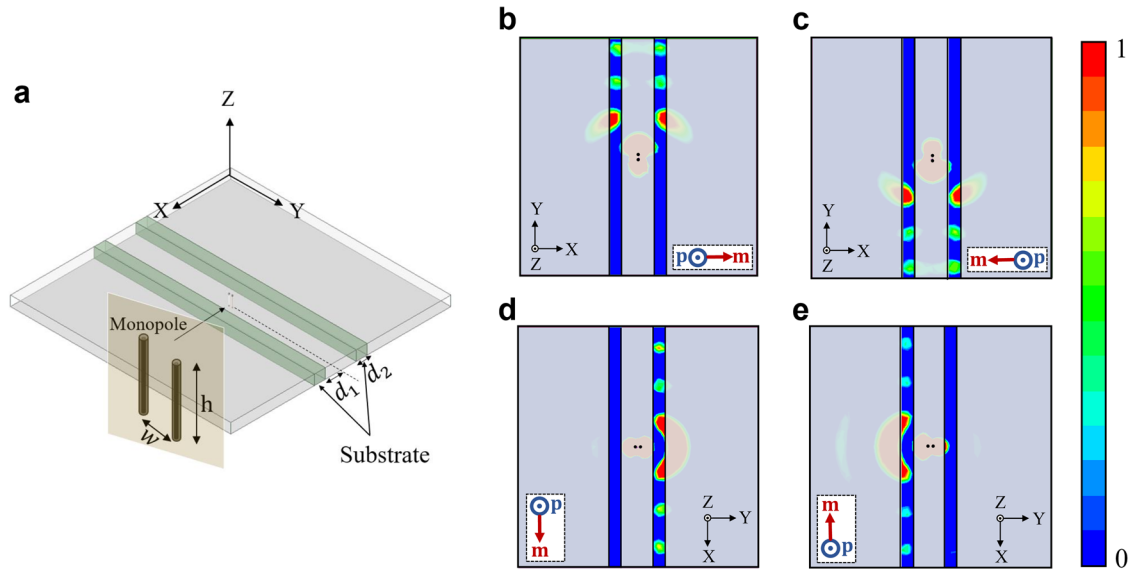
for the Janus source. Thus, by properly tuning  $I_0$  and  $\Delta\psi$ , we can actively excite the electric / magnetic dipole, Huygens and Janus sources within a 2D PPW environment.

Fig. 1b, c give the Argand diagram for Huygens source and Janus source respectively. The Huygens source, depicted in Fig. 1b, features symmetrically placed  $I_{aH}$  and  $I_{bH}$  around the real axis, resulting in the 90-degree phase shifted  $I_E$  (in blue) and  $I_M$  (in red). Equation (2) reveals a 90-degree separation between  $I_E$  and  $\mathbf{p}$ , allowing the creation of in-phase  $\mathbf{p}$  and  $\mathbf{m}$ . The Huygens source is then formed by determining  $\Delta\psi_H$  using Eq. (7). In Fig. 1c, the Janus source is presented.  $I_{aj}$  and  $I_{bj}$  are positioned along the real axis to create in-phase  $I_E$  and  $I_M$ . Due to the 90-degree difference between  $I_E$  and  $\mathbf{p}$ ,  $\mathbf{p}$  and  $\mathbf{m}$  become 90 degrees out of phase, signifying the formation of the Janus source.

We emphasize that the TCF is a realistic source that can be directly implemented with a microwave circuit. In<sup>11</sup> we experimentally demonstrated a simpler version of the TCF as a Huygens source along a metallic boundary. For the TCF in this work, we will excite the filaments by connecting them to co-axial cables from one side of the PPW. The proper current feeds can be straightforwardly generated by using an asymmetric power splitter and a meander line phase-shifter. We will report more details in the experiment section of this paper.

As shown in Fig. 1a, two currents  $I_a$  and  $I_b$  in z-direction comprise the active sources in this PPW environment. The current sources are excited as lumped ports where the port impedance is tuned to minimize reflection for a single TCF. This ensures the power delivered to the filament is radiated into the PPW. After we have optimized the port impedance, we excite the ports according to Eqs. (6) – (8) to generate electric dipole, Huygens source and Janus source excitations respectively. It should be noted that the excitation loaded to the ports does not affect the impedance matching results and the efficiency of the power delivered to the PPW can reach 90.61%, 94.78% and 94.78% for the electric dipole, the Huygens source and the Janus source respectively. The specifics of the efficiency computation are provided in Supplementary Note 2. Fig. 1d–f show the simulated  $|\mathbf{E}|$  field distributions associated with these three excitations. To compare with theory, we also show, in Fig. 1g–i, the simulated and calculated radiation patterns along the principal (xy) plane for an electric dipole, a Huygens source and a Janus source. Here the blue curves illustrate the radiation patterns calculated from the superposition of infinitesimal electric and magnetic dipoles with the requisite amplitudes and phases, within a 3D free-space environment. The dipole orientations of each case are labelled onto the radiation patterns. The red curves are the simulated “radiation” patterns (i.e. waves travelling outwards on the xy-plane within the infinite PPW waveguide). We can see that the simulated results are consistent with the calculated results. As expected, the electric dipole radiates omnidirectionally on the xy-plane, the Huygens source shows unidirectional radiation into the +y-direction, and the Janus source yields a quasi-isotropic radiation with about 3 dB variation across the angles, achieving maximum radiation in the  $\pm y$ -directions and minimum radiation (with roughly 70% field strength) in the  $\pm x$ -directions. Slight disagreements for the radiation of the Huygens source can be observed in Fig. 1h: this is understandable as the fields calculation is performed for a 3D infinitesimal source while simulation is performed for a 2D environment. Notwithstanding this, an agreement in the general radiation trend is observed. These results, particularly the agreement between Fig. 1f, i, validate our generation of the active Janus source using the TCF structure in this 2D PPW environment. Further, it shows that the 2D active sources demonstrated hereby attain very similar radiation characteristics as their 3D counterparts do in free space, along the principal plane. This makes our findings here directly applicable to 3D active sources in a free-space environment.

Moreover, we investigate the near-field coupling properties of the active Huygens and Janus sources using the setup shown in Fig. 2a, following previous works on the passive directional sources<sup>5,19,34</sup>. Depending on the characteristics of the source excitation, the electromagnetic near-fields produced exhibit a strong directional preference for coupling to the waveguides. In Fig. 2b, c, the directionality of the excited waveguide modes is depicted when the Huygens source is excited to radiate in the +y and -y directions, respectively. Similarly, Fig. 2d, e show the directionality of the



**Fig. 2 | Active Janus and Huygens sources' near-field directionality.** **a** A diagram of the source in parallel plate waveguide (PPW) with two substrates.  $\epsilon_r$  (substrate) = 3,  $d_1 = 60$  mm,  $d_2 = 50$  mm. **b, c** Simulated coupling directionality for the Huygens

source, toward the **(b)** +y and **(c)** -y directions. **d, e** Simulated coupling directionality for the Janus source, toward the **(d)** +y and **(e)** -y directions. In subfigures **(b–e)** the normalized  $|E|$  is shown.

excited waveguide modes when the Janus source is excited to direct near-field coupling to the +y and -y directions, respectively. The near-field directionality exhibited by the Huygens and Janus sources agree with those produced with ideal sources<sup>5</sup>. Further, we show that the near-field directionalities of the Huygens and Janus sources can be flexibly flipped through interchanging the excitation, from  $\{I_a, I_b\}$  to  $\{I_b, I_a\}$ , as shown in Fig. 2c compared to Fig. 2b, and in Fig. 2e compared to Fig. 2d. The essential reason for this is that this transformation preserves the direction of  $\mathbf{p}$  and flips the direction of  $\mathbf{m}$  (as can be seen from Eqs. (1) and (2)), and thus it flips the direction of  $\mathbf{p} \times \mathbf{m}$ , i.e., near-field directionality. The achievement of both the far-field radiation pattern and the near-field directionality strongly indicates the successful construction of an active Janus source within the 2D PPW environment.

We summarize the near-field and far-field directionalities of the electric dipole, the Huygens source and the Janus source in Table 1. It can be seen that both the Huygens and Janus sources are directional in the near field. However, in the far-field, the Huygens source remains directional while Janus source is quasi-isotropic. This distinction positions the Janus source as particularly promising for building a MIMO system.

**Near-field mutual coupling suppression with active Janus sources**

Having successfully generated the Janus source, we leverage its distinctive near-field directionality to reduce coupling between two closely spaced sources. Here, we introduce the electric dipole because, in most integrated systems, each cell is an independent electric dipole or magnetic dipole. Hence, we take as reference the mutual coupling between closely-spaced electric dipoles to characterize the mutual coupling between the three different active sources under consideration. First, we construct two active

sources shown in Fig. 3a based on the TCF model. All dimensions are the same as the TCF of Fig. 1a. To investigate the mutual coupling between two such sources, we separate them by a center-to-center distance  $d$  along the y-direction. Specifically, we vary  $d$  from  $0.08\lambda_0$  to  $0.24\lambda_0$  at an interval of  $0.04\lambda_0$  to investigate the mutual coupling in the near-field. The excitation of the pair of active sources  $\{I_{1aN}, I_{1bN}\}$  and  $\{I_{2aN}, I_{2bN}\}$  are found from Eqs. (6) - (8). Here  $N = E, H, J$  represent the electric dipole, Huygens source and Janus source respectively, and the subscripts 1 and 2 denote the first and second source. Notably, the two sources are identical, i.e.,  $I_{1a} = I_{2a} = I_a$ ;  $I_{1b} = I_{2b} = I_b$ . To suppress coupling between the two sources for the Huygens and Janus sources, one should orient the sources such that their near-field directionalities are facing away from each other. The source geometry is shown in Fig. 3a. Through properly tuning the  $\{I_{1a}, I_{1b}\}$  and  $\{I_{2a}, I_{2b}\}$ , we can generate the two Huygens and Janus sources for which the near-field directionalities ( $\mathbf{p} \times \mathbf{m}$ ) are in the -y and +y directions, respectively.

To characterize the mutual coupling between Sources 1 and 2, we design the RF circuit shown in Fig. S1a, that feeds both sources with a single port. The circuit contains a Wilkinson power splitter that splits the incident wave into the correct amplitude ratio of  $|I_a|$  and  $|I_b|$ . Thereafter, the branch with current amplitude  $I_b$  is meandered to achieve the required phase shift  $\Delta\psi$ . This simple feed network is quite common in microwave circuit design. Here it is theoretically modelled by its scattering matrix  $[S_{WPS}]$  (see Supplementary Note 3). Two such scattering matrices connect to Sources 1 and 2. They are combined, using microwave network theory, with a scattering matrix  $[S_{PPW}]$  obtained from full-wave simulation representing the port relationships when the two TCF sources are placed within the PPW environment. Supplementary Note 3 explains this procedure in detail. The combined system can now be described by its own scattering matrix. In particular, the parameter  $S_{total,21}$  denotes the ratio of the output wave at Port 2 to the input wave at Port 1, which thus characterizes the mutual coupling between the two sources. We also present in Table S1 (see Supplementary Note 2) the efficiency delivered to the PPW as the separation  $d$  changes. We observe that the system is highly efficient. This gives the foundation to investigate the mutual coupling suppression achievable with these specialised sources.

Using this formulation, we investigate the mutual coupling within for two TCFs separated at distance  $d$  within the PPW environment. A strength of our simulation method is that it requires only one full-wave simulation for each separation distance. We sweep the phase difference  $\Delta\psi$  and the amplitude  $|I_a|$  (the corresponding  $|I_b|$  is thus

**Table 1 | Summary of near-field and far-field directionalities properties**

	Near-field	Far-field
Dipole	Omnidirectional	Omnidirectional
Huygens Source	Directional	Directional
Janus Source	Directional	Quasi-isotropic

Summary of the near-field and far-field directionalities (on the xy-plane) of the dipole, the Huygens source and the Janus source.

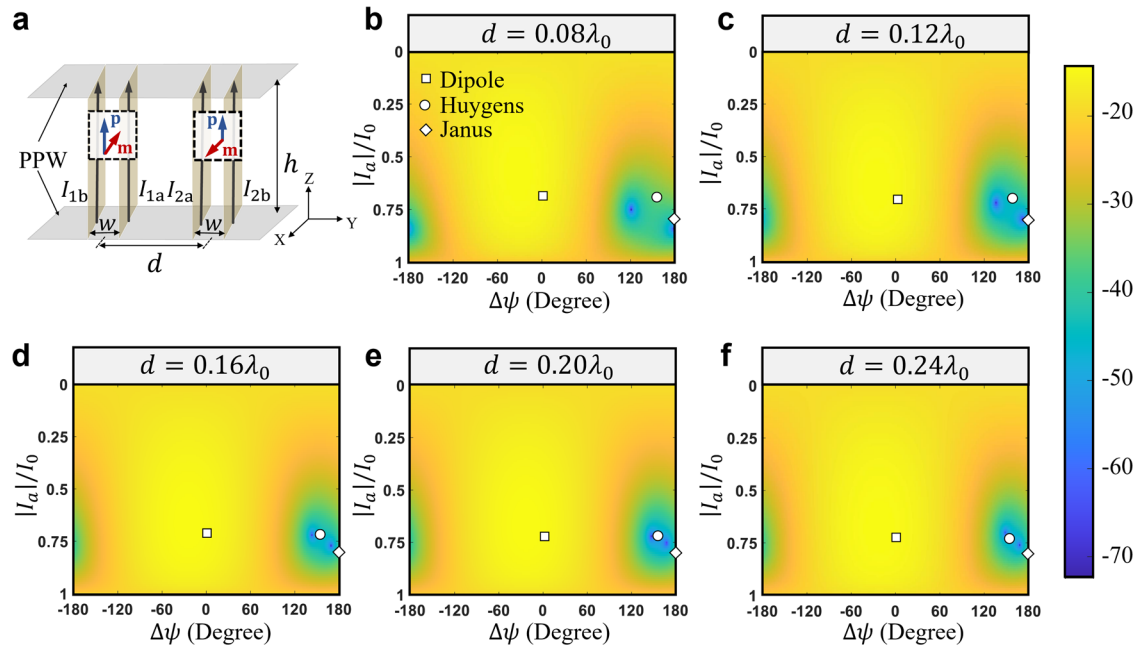


**Fig. 3 | Simulated coupling coefficient plot of two electric dipoles, Huygens sources and Janus sources.** **a** A diagram of two active sources within the parallel plate waveguide (PPW).  $h = 0.12\lambda_0$ ,  $w = 0.04\lambda_0$ ,  $d$  varies from  $0.08\lambda_0$  to  $0.24\lambda_0$  in increments of  $0.04\lambda_0$ . The simulations are performed at 800 MHz. Coupling

coefficient (dB) colour plot of **(b)**  $d = 0.08\lambda_0$ , **(c)**  $d = 0.12\lambda_0$ , **(d)**  $d = 0.16\lambda_0$ , **(e)**  $d = 0.2\lambda_0$ , **(f)**  $d = 0.24\lambda_0$  as a function of filament excitation ratios. Filament excitation ratios representing the dipole, Huygens and Janus sources are marked with squares, circles and rhombuses respectively.

**Table 2 | Simulated and measured coupling coefficients for two closely-spaced sources**

		$d = 0.08\lambda_0$	$d = 0.12\lambda_0$	$d = 0.16\lambda_0$	$d = 0.20\lambda_0$	$d = 0.24\lambda_0$
Dipole	Simulated	-13.08	-14.81	-15.95	-17.01	-17.66
	Measured	-12.95	-15.27	-15.17	-17.38	-19.20
Huygens Source	Simulated	-32.58	-42.64	-50.02	-55.96	-56.16
	Measured	-37.41	-39.33	-39.21	-41.47	-48.53
Janus Source	Simulated	-38.52	-44.59	-45.23	-45.32	-46.64
	Measured	-38.63	-40.14	-39.74	-42.45	-39.51

The simulated and measured coupling coefficients (dB) of the dipole, the Huygens source and the Janus source with separation  $d$  (the distance between two sources) changing from  $0.08\lambda_0$  to  $0.24\lambda_0$  in increments of  $0.04\lambda_0$ .

$|I_b| = \sqrt{|I_0|^2 - |I_a|^2}$  by modifying  $[S_{Feed}]$  to observe the mutual coupling for all possible combinations of  $\{|I_a|, |I_b|, \Delta\psi\}$ , including the electric dipole ( $(\frac{1}{\sqrt{2}}I_0, \frac{1}{\sqrt{2}}I_0, 0^\circ)$ ), Huygens source ( $(\frac{1}{\sqrt{2}}I_0, \frac{1}{\sqrt{2}}I_0, 165^\circ)$ ) and Janus source ( $(0.79I_0, 0.61I_0, 180^\circ)$ ). The excitation parameters for all sources are found from Eqs. (6) – (8). As an example, Fig. 3b shows the variation in mutual coupling with varying  $\Delta\psi$  and  $|I_a|$ , for  $d = 0.08\lambda_0$ . The conditions for the electric, Huygens and Janus sources are labelled. It can be observed that the region with low coupling coefficients are concentrated in the lower right region due to the presence of two mutual coupling nulls. Both the Huygens source (denoted by a circle marker) and the Janus source (denoted by a diamond marker) are in within the vicinity of this low-coupling region, hence they experience much weaker coupling compared to a pair of dipole sources. At this distance the mutual coupling between the Huygens and Janus source pairs are reduced by 19.5 dB and 25.44 dB respectively compared to the dipole source pair.

Likewise, Fig. 3b–f show the mutual coupling for all source pairs for distances from  $0.08\lambda_0$  to  $0.24\lambda_0$  at intervals of  $0.04\lambda_0$ . We observe that as  $d$  increases, the weakly coupled region remains within the lower right corner of the 2D colour map, and gradually moves closer to the location

of the Huygens source. Across all distances, the Huygens and Janus source are always in the weakly coupled region and the coupling suppression is significantly better than that of the electric dipole. Table 2 plots the coupling coefficients of the three different sources as a function of  $d$ . In terms of the simulated results, the coupling between two Huygens source pair is suppressed by more than 30 dB (1000 ×) compared the dipole source pair for  $d \geq 0.16\lambda_0$ . The coupling between the Janus source pair is suppressed by around 29 dB (794 ×) compared the dipole source pair for  $d \geq 0.16\lambda_0$ . In both cases, significant mutual coupling reduction is achieved using Huygens and Janus source pairs. It can be seen that the Huygens source pair achieves stronger suppression with increasing separation distance, while the Janus source pair seems to achieve a steady suppression level from  $d = 0.12\lambda_0$  to  $d = 0.24\lambda_0$ . Beyond this distance, the trend continues for the Huygens source pair while the Janus source pair ceases to produce strong coupling suppression. This can be explained by the fact that the Huygens source exhibits both near- and far-field directionality while the Janus source exhibits near-field directionality but is quasi-isotropic in the far-field.

**Experimental demonstration**

We proceed to experimental verification. A diagram of the experimental setup is shown in Fig. 4. Fig. 5b–f plot the measured coupling

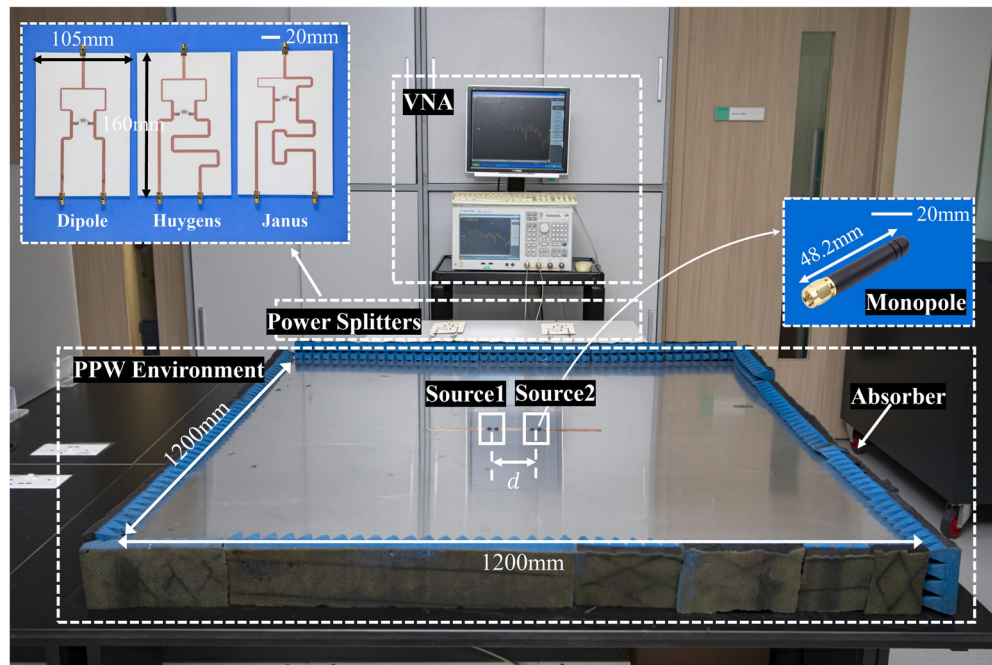


**Fig. 4 | Experiment setup.** A photo of the experimental apparatus, showing the parallel plate waveguide (PPW) environment, monopole used as the practical current, power splitters and the vector network analyzer (VNA). Scale bars are shown in the insets for the power splitters and the monopole.

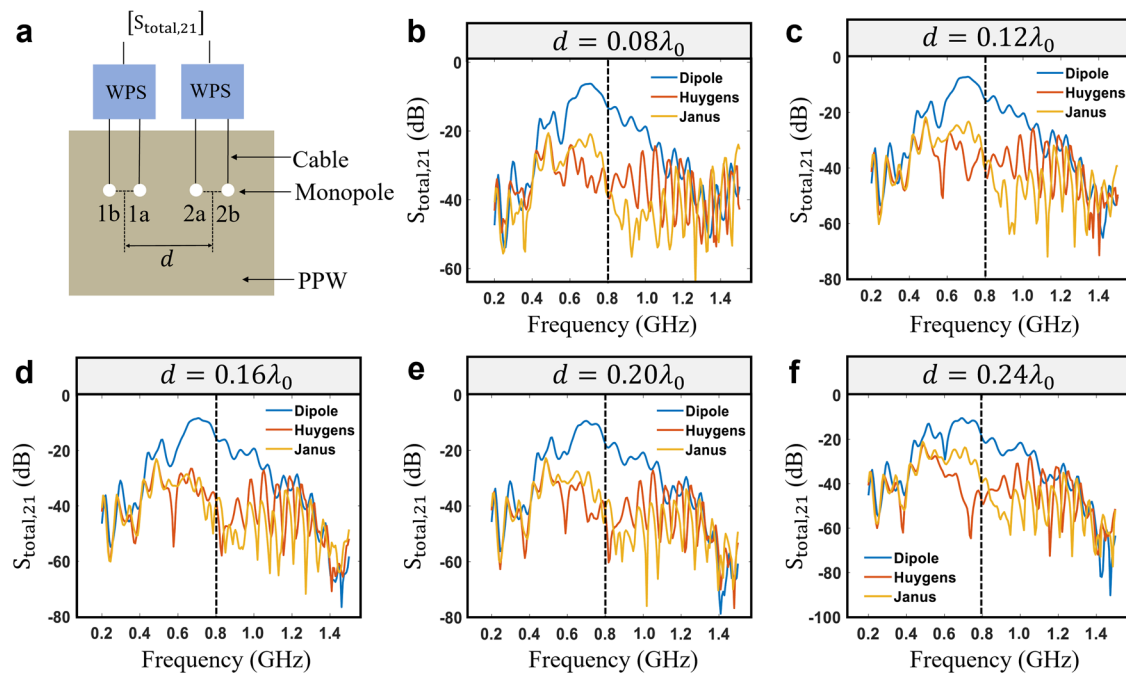


**Fig. 5 | Measured coupling coefficients.** **a** A schematic of the experiment structure, including Wilkinson power splitter (WPS), cable, monopole and parallel plate waveguide (PPW). Experimental mutual coefficient strength ( $S_{total,21}$ ) as a function of frequency for **(b)**  $d = 0.08\lambda_0$ , **(c)**  $d = 0.12\lambda_0$ , **(d)**  $d = 0.16\lambda_0$ , **(e)**  $d = 0.20\lambda_0$ , **(f)**  $d = 0.24\lambda_0$ .

coefficient as functions of frequency for different values of  $d$ . Table 2 shows the measured coupling coefficients for 800 MHz. The measured results show excellent agreement with the simulation: all coupling coefficients obtained from experiment and simulation agree to within 1% of the incident power. Minor differences may arise from losses during the experiment (e.g., cable, connector, and designed power splitter) and the absorber’s imperfection. For all separation

distances, mutual coupling is clearly suppressed for the Huygens and Janus sources pairs compared to the electric dipole source pair: Janus source pair achieves a suppression level exceeding 25 dB ( $> 316\times$ ) for all distances measured, while the Huygens source pair achieves a suppression level of 20–25 dB (100 to 316 $\times$ ) for distances up to  $0.20\lambda_0$ , and a suppression level approaching 30 dB (for 1000 $\times$ ) for  $d = 0.24\lambda_0$ . The mutually coupled power for Janus source pair is

lower than Huygens source pair for  $d = 0.08\lambda_0$  and  $d = 0.12\lambda_0$ , but at higher separating distances the Huygens source pair shows a stronger suppression in mutual coupling, consistent with observations from full-wave simulation. It is therefore clear that both Huygens and Janus sources can serve as good candidates in applications requiring low inter-element coupling; further, the Janus source's ability to achieve strongly suppressed mutual coupling while featuring a quasi-isotropic far-field gives points to intriguing application potential as antennas for compact MIMO systems.

## Conclusion

In this paper we have demonstrated the first realistic active Janus source and reported near-field mutual coupling suppression between a pair of such active Janus sources. We design a simple, realistic active Janus source based on a succinct PPW structure. The presented model can function as all three sets of fundamental dipolar sources (electric/magnetic dipole, Huygens source, and Janus source) under the right excitation, thereby allowing us to investigate the near-field mutual coupling when these fundamental source pairs are in close proximity to each other. The simulation and experiment results show a many-fold (up to 1000 times) suppression of coupling in the Huygens and Janus source pairs when compared to a pair of electric dipoles at similar separation from each other. The findings in this work open door to the exploration of these directional sources in densely packed systems where coupling between cells has imposed limitations. More interestingly, since the Janus source is quasi-isotropic in the far-field, the significant near-field coupling suppression positions it as a good candidate for future compact MIMO antennas design.

## Methods

### Numerical simulations

All the full-wave simulations are performed with Ansys HFSS. We adopt the frequency of 800 MHz ( $\lambda_0 = 375$  mm) for simulation (and eventual experiment) due to the ease of fabricating precise TCF elements and availability of SMA adaptors and monopole antennas at this frequency. As shown in Fig. 1a, the key TCF dimensions are  $h = 0.12\lambda_0$ , and  $w = 0.04\lambda_0$ . The PPW has a size of  $l = 4\lambda_0 = 1500$  mm; it is terminated by a radiation boundary to simulate infinite wave propagation. We place the TCF at the middle of the PPW and observe the spatial field distributions inside the PPW. The port impedance is swept to reduce reflection for a single TCF since the current sources are excited as lumped ports. This ensures that the current sent to the filament is also sent out into the PPW.

Next, we simulate the geometry of Fig. 2a to observe the near-field directionality of the active TCF source. Similar to the waveguide coupling topology in<sup>5</sup>, two dielectric waveguides are positioned at a sub-wavelength distance  $d_1$  from the active source. For the Huygens source, the dielectric waveguides are symmetric with respect to the origin along the y-axis, while for the Janus source, symmetry is along the x-axis. The change in waveguide direction is necessitated by the near-field directionality of the Huygens and Janus sources. Further, it can be seen from Fig. 2b–e that the directions of  $\mathbf{p}$  and  $\mathbf{m}$  in each case determines its near-field directionality ( $\mathbf{p} \times \mathbf{m}$ , i.e. the  $\pm y$  direction).

Regarding the two-Janus-source system shown in Fig. 3a, we obtain from the full-wave simulation a four-port scattering matrix  $[S_{PPW}]$ , which characterizes the input-output information involving the four source ports (two ports per TCF source). We then calculate the coupling coefficient assuming the usage of ideal Wilkinson power splitters. More details are given in the Supplementary Note 3.

### Experiments

Two 1200 mm  $\times$  1200 mm square aluminum plates separated at a sub-wavelength height  $h = 45$  mm form the top and bottom plates of the PPW. Microwave absorbers are placed at the PPW boundary to prevent reflection from the edge of the PPW. The active sources are built using

monopole antennas as the driven elements. An array of holes was drilled in both aluminum plates for the insertion of the monopoles. The corresponding passive lossless microwave feed circuits for each of the three sources — electric dipole, Huygens source and Janus source are designed to achieve the specific excitation weights necessary to implement the sources according to Eqs. (6) – (8). Port 1 of a Keysight E5071C Vector Network Analyzer (VNA) provides the input power to microwave feed network 1 with its two output ports exciting source 1 (electric dipole, Huygens, Janus) at prescribed excitation amplitudes and phases. Similarly, the VNA's Port 2 provides the input power to microwave feed network 2, with its two output ports exciting the dipole source 2 (dipole, Huygens, Janus) as appropriate (refer to Fig. 5a). The coupling coefficients ( $S_{total,21}$ ) are then measured by the VNA.

### Data availability

The authors declare that all data supporting the findings of this study are available within the paper and its Supplementary Information files. Additional data related to this paper are available from the corresponding authors upon reasonable request.

### Code availability

The codes and simulation files that support the plots and data analysis in this paper are available from the corresponding authors upon reasonable request.

Received: 30 October 2023; Accepted: 20 February 2024;

Published online: 09 March 2024

## References

1. Fresnel, A. Mémoire sur la diffraction de la lumière. *Impr. Imp.* **1**, 247363 (1870).
2. Kirchhoff, G. Zur Theorie der Lichtstrahlen. *Ann. der Phys.* **254**, 663695 (1883).
3. Love, A. E. H. I. The integration of the equations of propagation of electric waves. *Philos. Trans. R. Soc. Lond. Ser. Contain. Pap. Math. Phys. Character* **197**, 1–45 (1901).
4. Schelkunoff, S. A. Some equivalence theorems of electromagnetics and their application to radiation problems. *Bell Syst. Tech. J.* **15**, 92–112 (1936).
5. Picardi, A. V., Rodríguez-Fortuño, F. J. & Picardi, M. F. Janus and Huygens Dipoles: Near-Field Directionality Beyond Spin-Momentum Locking. *Phys. Rev. Lett.* **120**, 117402 (2018).
6. Kuznetsov, A. I., Miroshnichenko, A. E., Brongersma, M. L., Kivshar, Y. S. & Luk'yanchuk, B. Optically resonant dielectric nanostructures. *Science* **354**, aag2472 (2016).
7. Permyakov, D. et al. Probing magnetic and electric optical responses of silicon nanoparticles. *Appl. Phys. Lett.* **106**, 171110 (2015).
8. Pfeiffer, C. & Grbic, A. Metamaterial Huygens' surfaces: tailoring wave fronts with reflectionless sheets. *Phys. Rev. Lett.* **110**, 197401 (2013).
9. Chen, M., Kim, M., Wong, A. M. H. & Eleftheriades, G. V. Huygens' metasurfaces from microwaves to optics: a review. *Nanophotonics* **7**, 1205–1231 (2018).
10. Fan, K. et al. Phototunable Dielectric Huygens' Metasurfaces. *Adv. Mater.* **30**, 1800278 (2018).
11. Wong, A. M. H. & Eleftheriades, G. V. Active Huygens' Box: arbitrary electromagnetic wave generation with an electronically controlled metasurface. *IEEE Trans. Antennas Propag.* **69**, 1455–1468 (2021).
12. Luk, K.-M. & Wong, H. A new wideband unidirectional antenna element. *Int. J. Micro. Opt. Technol.* **1**, 35–44 (2006).
13. Ge, L. & Luk, K. M. A low-profile magneto-electric dipole antenna. *IEEE Trans. Antennas Propag.* **60**, 1684–1689 (2012).
14. Ziolkowski, R. W. Low profile, broadside radiating, electrically small Huygens source antennas. *IEEE Access* **3**, 2644–2651 (2015).

15. Ziolkowski, R. W. Using Huygens multipole arrays to realize unidirectional needle-like radiation. *Phys. Rev. X* **7**, 031017 (2017).
16. Wu, T., Baron, A., Lalanne, P. & Vynck, K. Intrinsic multipolar contents of nanoresonators for tailored scattering. *Phys. Rev. A* **101**, 011803 (2020).
17. Zhong, Y. et al. Toggling near-field directionality via polarization control of surface waves. *Laser Photonics Rev.* **15**, 2000388 (2021).
18. Picardi, M. F. et al. Integrated Janus dipole source for selective coupling to silicon waveguide networks. *Appl. Phys. Rev.* **9**, 021410 (2022).
19. Cheng, Y. et al. Directional dipole dice enabled by anisotropic chirality. *Proc. Natl Acad. Sci.* **120**, e2301620120 (2023).
20. Lin, X. & Zhang, B. Normal Doppler frequency shift in negative refractive-index systems. *Laser Photonics Rev.* **13**, 1900081 (2019).
21. Shi, X. et al. Superlight inverse Doppler effect. *Nat. Phys.* **14**, 1001–1005 (2018).
22. Jiang, Y., Lin, X., Low, T., Zhang, B. & Chen, H. Group-velocity-controlled and gate-tunable directional excitation of polaritons in graphene-boron nitride heterostructures. *Laser Photonics Rev.* **12**, 1800049 (2018).
23. Chen, X. et al. Broadband Janus scattering from tilted dipolar metagratings. *Laser Photonics Rev.* **16**, 2100369 (2022).
24. Tan, Q. et al. Broadband Spin-locked metasurface retroreflector. *Adv. Sci.* **9**, 2201397 (2022).
25. Huang, H.-F. & Huang, H.-M. Millimeter-wave wideband high efficiency circular Airy OAM multibeam with multiplexing OAM modes based on transmission metasurfaces. *Prog. Electromagn. Res.* **173**, 151–159 (2022).
26. Picardi, M., Zayats, A. & Rodríguez-Fortuño, F. Not every dipole is the same: The hidden patterns of dipolar near fields. *Europhys. N.* **49**, 14–18 (2018).
27. Picardi, M. F. et al. Experimental demonstration of linear and spinning Janus dipoles for polarisation- and wavelength-selective near-field coupling. *Light Sci. Appl.* **8**, 52 (2019).
28. Long, Y. et al. Symmetry selective directionality in near-field acoustics. *Natl Sci. Rev.* **7**, 1024–1035 (2020).
29. Long, Y. et al. Designing all-electric subwavelength metasources for near-field photonic routings. *Phys. Rev. Lett.* **125**, 157401 (2020).
30. Wei, L. & Rodríguez-Fortuño, F. J. Far-field and near-field directionality in acoustic scattering. *N. J. Phys.* **22**, 083016 (2020).
31. Wei, L. & Rodríguez-Fortuño, F. J. Momentum-Space Geometric Structure of Helical Evanescent Waves and Its Implications on Near-Field Directionality. *Phys. Rev. Appl.* **13**, 014008 (2020).
32. Jiang, Y., Lin, X. & Chen, H. Directional Polaritonic Excitation of Circular, Huygens and Janus Dipoles in Graphene-Hexagonal Boron Nitride Heterostructures. *Prog. Electromagn. Res.* **170**, 169–176 (2021).
33. Jiang, H. et al. Near-field Properties of Spin, Huygens and Janus Sources in a Narrow Sandwiched Structure. *J. Phys. B. Mol. Opt. Phys.* **55**, 155001 (2022).
34. Xue, B. & Wong, A. M. H. Active Janus and Huygens Sources: Achieving Near-field and Far-field Directionality Control. in 2022 IEEE International Symposium on Antennas and Propagation and USNC-URSI Radio Science Meeting (AP-S/URSI) 974–975 (2022).
35. Weber, J., Volmer, C., Blau, K., Stephan, R. & Hein, M. A. Miniaturized antenna arrays using decoupling networks with realistic elements. *IEEE Trans. Microw. Theory Tech.* **54**, 2733–2740 (2006).
36. Abdalla, M. A. & Ibrahim, A. A. Compact and closely spaced metamaterial MIMO antenna with high isolation for wireless applications. *IEEE Antennas Wirel. Propag. Lett.* **12**, 1452–1455 (2013).
37. Zhai, G., Chen, Z. N. & Qing, X. Mutual coupling reduction of a closely spaced four-element MIMO antenna system using discrete mushrooms. *IEEE Trans. Microw. Theory Tech.* **64**, 3060–3067 (2016).
38. Lin, K.-C., Wu, C.-H., Lai, C.-H. & Ma, T.-G. Novel dual-band decoupling network for two-element closely spaced array using synthesized microstrip lines. *IEEE Trans. Antennas Propag.* **60**, 5118–5128 (2012).
39. Tang, X., Qing, X. & Chen, Z. N. Simplification and Implementation of decoupling and matching network with port pattern-shaping capability for two closely spaced antennas. *IEEE Trans. Antennas Propag.* **63**, 3695–3699 (2015).
40. Venkatasubramanian, S. N., Li, L., Lehtovuori, A., Icheln, C. & Haneda, K. Impact of using resistive elements for wideband isolation improvement. *IEEE Trans. Antennas Propag.* **65**, 52–62 (2017).
41. Amin, F. et al. A Compact Quad-Element UWB-MIMO Antenna system with parasitic decoupling mechanism. *Appl. Sci.* **9**, 2371 (2019).
42. Li, M., Jiang, L. & Yeung, K. L. A novel wideband decoupling network for two antennas based on the Wilkinson power divider. *IEEE Trans. Antennas Propag.* **68**, 5082–5094 (2020).
43. Lee, J.-Y., Kim, S.-H. & Jang, J.-H. Reduction of mutual coupling in planar multiple antenna by Using 1-D EBG and SRR structures. *IEEE Trans. Antennas Propag.* **63**, 4194–4198 (2015).
44. Qamar, Z., Naeem, U., Khan, S. A., Chongcheawchamnan, M. & Shafique, M. F. Mutual coupling reduction for high-performance densely packed patch antenna arrays on finite substrate. *IEEE Trans. Antennas Propag.* **64**, 1653–1660 (2016).
45. Xu, S., Zhang, M., Wen, H. & Wang, J. Deep-subwavelength decoupling for MIMO antennas in mobile handsets with singular medium. *Sci. Rep.* **7**, 12162 (2017).
46. Sun, L., Li, Y., Zhang, Z. & Wang, H. Self-Decoupled MIMO antenna pair with shared radiator for 5G Smartphones. *IEEE Trans. Antennas Propag.* **68**, 3423–3432 (2020).
47. Lai, Q. X., Pan, Y. M., Zheng, S. Y. & Yang, W. J. Mutual coupling reduction in MIMO Microstrip Patch Array Using TM<sub>10</sub> and TM<sub>02</sub> Modes. *IEEE Trans. Antennas Propag.* **69**, 7562–7571 (2021).
48. Wong, A. M. H. & Eleftheriades, G. V. A simple active Huygens source for studying waveform synthesis with Huygens metasurfaces and antenna arrays. in 2015 IEEE International Symposium on Antennas and Propagation & USNC/URSI National Radio Science Meeting 1092–1093 (IEEE, 2015).
49. Oyesina, K. A. & Wong, A. M. Metasurface-enabled cavity antenna: Beam steering with dramatically reduced fed elements. *IEEE Antennas Wirel. Propag. Lett.* **19**, 616–620 (2020).

## Acknowledgements

The work described in this paper was supported by the Government of Hong Kong's RGC GRF Award, grant 11204522.

## Author contributions

A.M.H.W. conceived the original idea. A.M.H.W. and B.X. did the theoretical analysis and numerical simulations. B.X. and K.A.O. performed the experiments. B.X. and A.M.H.W. drafted the manuscript. A.M.H.W. supervised the project. All authors participated in discussions and reviewed the manuscript.

## Competing interests

The authors declare no competing interests.

### Additional information

**Supplementary information** The online version contains supplementary material available at <https://doi.org/10.1038/s42005-024-01569-x>.

**Correspondence** and requests for materials should be addressed to Alex M. H. Wong.

**Peer review information** *Communications Physics* thanks Bingxiang Li, Francisco Rodríguez-Fortuño and the other, anonymous, reviewer(s) for their contribution to the peer review of this work.

**Reprints and permissions information** is available at <http://www.nature.com/reprints>

**Publisher's note** Springer Nature remains neutral with regard to jurisdictional claims in published maps and institutional affiliations.

**Open Access** This article is licensed under a Creative Commons Attribution 4.0 International License, which permits use, sharing, adaptation, distribution and reproduction in any medium or format, as long as you give appropriate credit to the original author(s) and the source, provide a link to the Creative Commons licence, and indicate if changes were made. The images or other third party material in this article are included in the article's Creative Commons licence, unless indicated otherwise in a credit line to the material. If material is not included in the article's Creative Commons licence and your intended use is not permitted by statutory regulation or exceeds the permitted use, you will need to obtain permission directly from the copyright holder. To view a copy of this licence, visit <http://creativecommons.org/licenses/by/4.0/>.

© The Author(s) 2024